Computers and Concrete, Vol. 9, No. 1 (2012) 21-33
DOI: http://dx.doi.org/10.12989/cac.2012.9.1.021

A numerical study on the damage of projectile impact on concrete targets

Gang Lu*[1], Xibing Li[2] and Kejin Wang[3]

[1]*Shaw Stone & Webster Nuclear, Stoughton, MA, USA 02072*
[2]*School of Resources and Safety Engineering, Central South University, Changsha, China 410083*
[3]*National Concrete Pavement Center, Iowa State University, Ames, IA, USA 50010*

(Received April 7, 2010, Revised February 25, 2011, Accepted April 8, 2011)

Abstract. This paper presents the numerical simulation of the rigid 12.6 mm diameter kinetic energy ogive-nosed projectile impact on plain and fiber reinforced concrete (FRC) targets with compressive strengths from 45 to 235 MPa, using a three-dimensional finite element code LS-DYNA. A combined dynamic constitutive model, describing the compressive and tensile damage of concrete, is implemented. A modified Johnson_Holmquist_Cook (MJHC) constitutive relationship and damage model are incorporated to simulate the concrete behavior under compression. A tensile damage model is added to the MJHC model to analyze the dynamic fracture behavior of concrete in tension, due to blast loading. As a consequence, the impact damage in targets made of plain and fiber reinforced concrete with same matrix material under same impact velocities (650 m/s) are obtained. Moreover, the damage distribution of concrete after penetration is procured to compare with the experimental results. Numerical simulations provide a reasonable prediction on concrete damage in both compression and tension.

Keywords: concrete; material model; numerical simulation; projectile penetration.

1. Introduction

Missile barriers and protective structures are widely used in nuclear facilities to withstand and absorb missile impact loads to prevent damage to safety-related components. The design of missile barrier includes using the empirical formula, normally modified National Defense Research Committee (NDRC) formula, to determine the penetration depth, perforation and scabbing thicknesses. As the most widely used construction material in nuclear facilities, concrete has been widely studied for its impact response, which differs from that under static loading. Local damage in concrete caused by projectile impact depends on a variety of characters, such as impact velocity, mass, geometry, and material properties of the fragments, as well as concrete properties (Zhang 2007).

When concrete is subjected to an impact loading by fragments, a crater is usually produced as a result of the concentrated forces on the surface of the concrete. These forces are transmitted inwards, thereby crushing the concrete in the crater region. Even though impact on concrete targets and cratering has been widely studied, little has been published on a front face spall (Collins *et al.* 2007). Most of the previous studies on projectile impact on concrete target focused on the penetration depth and indicated that the penetration depth is dependent upon the compressive strength of the

* Corresponding author, Ph.D., E-mail: ganglu9@gmail.com

target concrete (Luk 1987, Forrestal 1988, Degen 1980, Clifton 1982, Hanchak 1992, Dancygier 1996, 2002, O'Neil 1999, Bindiganavile 2002, Zhang *et al.* 2005, Lok 2003). Some recent studies on plain and fiber reinforced concrete found that the penetration depth in the concrete target was reduced with an increase in the compressive strength of the concrete; however, further increase in the compressive strength could not reduce the depth of penetration, and the crater diameter is mainly dependant upon the tensile and shear strengths of the concrete target (Zhang 2005, 2007, Lok 2003). These studies also found that ductility of steel fiber reinforced concrete was noticeably absent in the dynamic tests at high strain rate (Lok 2003). The incorporation of fibers in concrete reduced the crater diameter and crack propagation, but did not have a significant effect on penetration depth (Zhang 2005, 2007). Thus, both compressive and tensile strengths of concrete play important roles in penetration resistance of concrete targets.

With recent developments in computational and experimental techniques, new constitutive models for the numerical simulation to predict the dynamic behavior of a concrete target to close-in blast and projectile impact have been widely studied. Among these material models, the widely accepted are Holmquist-Johnson-Cook model (HJC), Taylor-Chen-Kuszmaul model (TCK) and Riedel-Thoma-Hiermaier model (RTH). The HJC model considered most of the important material parameters of concrete, such as hydrostatic pressure, strain rate and compressive damage, to describe the compressive damage of concrete under large strain and high strain rates (Holmquist 1993). It represents a good compromise between simplicity and accuracy for large-scale computations. The HJC model is incorporated into the LS-DYNA code and has been widely accepted in numerical simulations of the dynamic responses of concrete structures (LS-DYNA 1999). However, the tensile damage of concrete is not considered in the HJC model. The tensile behavior of concrete is simply considered through maximum tensile hydrostatic pressure. The strain rate affect is considered by using a dynamic increase factor (DIF), i.e. the ratio of dynamic-to-static strength versus strain rate on a semi-log scale. However, the DIF used in the HJC model is much lower than what is found from test results by other researchers and the author (Gebbeken 2000). Moreover, the strain rate effect on concrete tensile strength and concrete reloading are not considered. The crack propagation of concrete, due to tensile damage, cannot be predicted (Zhou 2008).

It is important to mention here that the HJC model only considered the effect of pressure and shear, which is in terms of the von Mises equivalent stress, and is not able to reflect the shear response accurately (Polanco-Loria *et al.* 2008). By using those commonly used material parameters in the HJC model, e.g. $A = 0.75$, $B = 1.65$ and $N = 0.75$, the uniaxial compression strength is overestimated by about 45%, and 450% for biaxial compressions strength (Polanco-Loria *et al.* 2008). To enhance the capability of the pressure-shear behavior for the HJC model, Polanco-Loria *et al.* (2008) modified the HJC model by introducing the influence of the third stress invariant to differentiate the tensile and compressive meridians. Moreover, a new DIF was applied to consider the strain rate effect. However, like the other models mentioned previously, the material parameters for concrete are very difficult to determine because the experimental test in the extreme condition is not easy to perform and accurate results are difficult to obtain, due to the limitations of the measurement method. Therefore, the strength model for the deviatoric portion was mainly based on the combination of static test results and the strain rate effect of concrete (Holmquist 1993, Riedel 1999). The parameters to determine the EOS are mainly based on static experimental results and assumptions on porous materials.

Different from the HJC model, the TCK model is a continuum damage model to characterize the dynamic fracture of concrete in tension by considering the tensile stress, micro crack density, and

volume strain. The TCK model is capable to predict the brittle tensile failure (scabbing) and the cracking growth of concrete (Taylor 1986). However, the dynamic compressive response of concrete material is simply described by an elastic-perfect plastic constitutive equation (Zhou 2008).

Riedel *et al.* (1999) modified the HJC model (RHT) by replacing its porous EOS model with Herrman's P-α, porous model, and by considering the stress tensor J_3 by building up the yield meridian plane with a cap, different tensile, and compressive meridians. However, the RHT model kept the strain rate effect and the damage variable similar to those in the HJC model.

Gebbeken and Ruppert (2000) modified the yield surface of the HJC model with different tensile and compressive meridians, and a shape function to define octahedral stresses in the deviatoric plane. The strain rate effect (up to 10^6/sec) and the damage were more comprehensively modeled. However, the DIF of RHT model still underestimated the strain rate effect in the high strain rate range. Recently, Leppänen (2006) improved the RHT model by using a different DIF for tension and bi-linear crack softening law. This parametric study confirmed cracking growth and scabbing of concrete in a penetration simulation are mainly influenced by the tensile strength, fracture energy, and strain rate in tension.

In this study modification was made to the original HJC model to enhance the strain rate effect. A DIF for dynamic compressive strength was proposed based on SHPB test results on plain and fiber reinforced concrete. A simple dynamic tensile damage model was developed and combined with the DIF enhanced HJC model. Less equations are needed to be integraled when volume increases. Previous experimental results (Zhang 2005, 2008, Lok *et al.* 2003) were used to determine the necessary material parameters and were used to compare with the results from numerical simulations.

2. Material model for concrete

In this study, the compressive damage of concrete is described by a modified HJC model. The modifications include: (1) a modified strain rate effect for compression, (2) simplified normalized equivalent stress equation, and (3) a simple, yet reliable, dynamic tensile damage model for concrete.

2.1 Strain rate effect

Over the past decades numerous works have been conducted on both theoretical and experimental studies of the strain rate effect on cement-based materials. Over the past decades, most of the dynamic failure criterions are obtained by the curve fitting of experimental data, and conversely, the physical mechanism and the mathematical expression of the strain rate effects is still far from fully understood (Cao and Chung 2002, Ou *et al.* 2010). Nowadays, two approaches to describe dynamic behavior of cement based materials are commonly accepted, and they are: 1) critical dynamic strength criterion, which handles dynamic failure strength of a cement based material by extension of material's static strength by a dynamic increase factor (DIF); and 2) the inertial effect and wave propagation mechanisms, which believes the dynamic failure strength of a material is not an intrinsic material property, but a computational characteristic. Most recently, a complete study on strain rate effect has been completed by Cotsovos and Pavloviæ (2008a, 2008b, 2008c). By using a quasi-static constitutive model as well as static material strength, they performed non-linear finite element analysis to study the behavior and failure of concrete specimens under dynamic load, and found that their results from numerical simulations were consistent with the published experimental

data. Based on their results they concluded that the effect of strain rate on the specimen's behavior reflects the effect of the inertia loads instead of a intrinsic material property. Therefore, the use of experimental data from dynamic tests to model constitutive behavior of concrete under dynamic loads is questionable (Cotsovos and Pavlović 2008a).

However, on the other hand, as a convenient format for implementation into numerical models DIF is still widely accepted to represent the strain rate effect on the dynamic behavior of concrete. Many empirical relations are available in the literature to estimate strain rate effect on the dynamic behavior of concrete (Malvar 1998). Particularly in this study, the DIF is still employed to represent the strain rate effect. This is because that both the SHPB test to investigate the strain rate effect, which is employed in this study to find the DIFs, and the projectile impact tests to study the concrete target responds to high velocity projectile impact, which are employed as real cases to be simulated in this study, were performed by the authors by using fiber reinforced concrete materials having similar properties (Lok 2003, Zhang 2005 and 2007). This can enhance ability of the model presented in this paper to produce accurate predictions. A summary of DIFs from previous studies (Schuler *et al.* 2006), together with the authors' experimental results obtained from a 75 millimeter Split Hopkinson Pressure Bar (SHPB) on both plain and steel fiber reinforced concrete samples (Lok 2003) is shown in Fig. 1. The static compressive strength of specimens varied between 70 N/mm^2 and 90 N/mm^2. Dynamic compressive and splitting tensile strengths of plain and fiber reinforced concrete specimens were obtained from 70 mm diameter by 140 mm long and 70 mm diameter by 70 mm long cylinders, respectively.

The strain rate considered in this study is in the wide range from the low value less than $10^{-5}s^{-1}$ to the high value about $1000s^{-1}$. New DIF functions for the compressive (CDIF) and tensile (TDIF) strength are developed and adopted in the present study. The empirical formulae are expressed as

$$CDIF = EXP(0.0046 \cdot \dot{\varepsilon}) \quad \text{for} \quad \dot{\varepsilon} \le 20s^{-1} \tag{1a}$$

$$CDIF = 0.4190 \times \dot{\varepsilon}^{0.3223} \quad \text{for} \quad 20s^{-1} < \dot{\varepsilon} < 1000s^{-1} \tag{1b}$$

and

$$TDIF = 1 \quad \text{for} \quad \dot{\varepsilon} \le 10^{-5}s^{-1} \tag{2a}$$

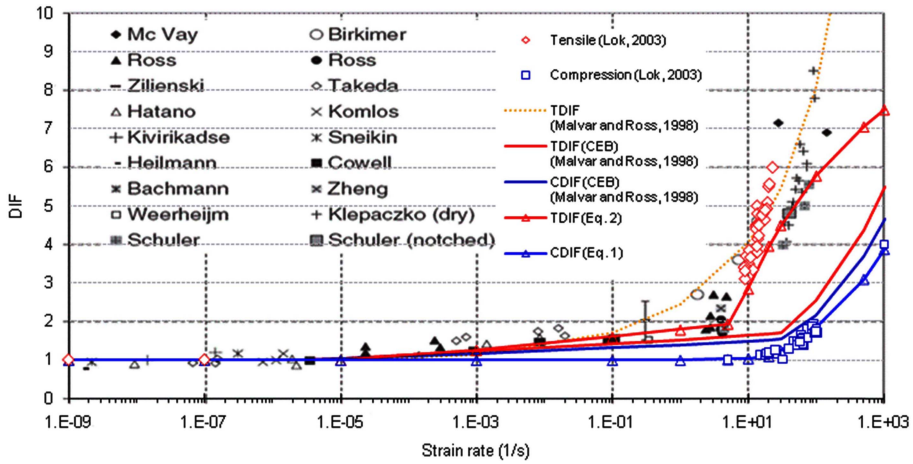

Fig. 1 DIF for tensile and compressive strength (Modified from Schuler *et al.* (2006))

$$TDIF = 1.7914 \times \dot{\varepsilon}^{0.0506} \quad \text{for} \quad 10^{-5} s^{-1} < \dot{\varepsilon} \leq 5 s^{-1} \tag{2b}$$

$$TDIF = 4.23 \times \ln(\ln \dot{\varepsilon}) - 0.68 \quad \text{for} \quad 5 s^{-1} < \dot{\varepsilon} \leq 1000 s^{-1} \tag{2c}$$

The strain rate value is cut off at 1000 s^{-1} to avoid overestimation of the strain rate effect. Thus, from the DIFs, the dynamic strength of concrete materials can be obtained.

2.2 The compressive damage model

In this study, a new strain rate dependence function, CDIF, given in Eqs. (1a) and (1b), was incorporated into the HJC model as shown in Eq. (3).

$$\sigma_{eq}^{*} = [A(1-D) + BP^{*N}][CDIF] \tag{3}$$

where σ_{eq}^{*} is the normalized equivalent stress given as $\sigma_{eq}^{*} = \sigma_{eq}/f_c'$, where σ_{eq} is the actual equivalent stress and f_c' is the quasi-static uniaxial compressive strength, P^* is the normalized pressure give by the actual hydrostatic pressure P and f_c' as $P^* = P/f_c'$, CDIF is the dimensionless dynamic increase factor of material given in Eqs. (1a) and (1b), A, B and N are material constants, and D is the internal compressive damage state variable and $0 \leq D \leq 1$. The damage for fracture is accumulated in a manner similar to that used in the original HJC model (Holmquist 1993)

$$D_c = \sum \frac{\Delta \varepsilon_p + \Delta \mu_p}{\varepsilon_p^f + \mu_p^f} \tag{4}$$

In this equation $\Delta \varepsilon_p$ and $\Delta \mu_p$ are the increments of equivalent plastic strain and plastic volumetric strain, respectively. Also, $\varepsilon_p^f + \mu_p^f = D_1(P^* + T^*)^{D_2}$ is the total plastic strain to fracture under a constant pressure, P. In this equation D_1 and D_2 are material constants. The concrete cannot experience any plastic strain when $P^* = -T^*$. Moreover, a third damage constant, $E_{fmin} = 0.01$, is used to suppress fracture by weak tensile waves (Holmquist 1993).

2.3 The tensile damage model

Numerous researches show that the mechanical response of concrete is mainly governed by the development of sub-scale cracks (Jan 1997, Suaris 1984), and damage of the concrete material is related to the gradual opening of these cracks. Normally, the damage based constitutive model takes account of damage evolution induced by the sub-scale crack development under tensile stress. And the tensile damage of the concrete materials can be demonstrated in the progressive degradation of the material stiffness.

The stress is correlated to strain with Young's modulus (E) and tensile damage (D) as

$$\sigma = E(1-D)\varepsilon \tag{5}$$

where σ and ε are tensile stress and strain, respectively. The tensile damage (D) is obtained from the volume of idealized penny-shaped cracks in the material as (Grady and Kipp 1980)

$$D = NV \tag{6}$$

where N is the number of cracks per unit volume and $V = 4/3\pi r^3$ is the spherical reign surrounding the penny-shaped crack of radius r.

From experimental observations conducted by the author (Zhang 2005, 2008, Lok 2003), it is clear that a concrete specimen fractures into a few large fragments when it is loaded at low strain rate. Conversely, the specimen breaks into many smaller fragments at high strain rate loading. Similar observations were reported by Shockey *et al.* (1974), Ross *et al.* (1996) for brittle materials such as rock, concrete and mortar.

The relationship between the average fragment size and the average strain rate was described by Ross *et al.* (1996). Smaller fragment size corresponds to smaller and more cracks developed in the damaged material. So, it is reasonable to suggest that the number of active cracks developed in the specimen is dependent on the strain rate at which the specimen is loaded; the higher the strain rate, the larger the crack number.

Physically, the shock loading sets up stress waves in the specimen. Such loading produces a more uniform strain field because parts of the concrete material remain loaded as the wave continues to propagate through the fractured specimen. In contrast, in static loading condition, the specimen is likely to be unloaded when a major crack is formed so that no other cracks can be further developed. Li and Gu (1994) further showed that high frequency components activate smaller cracks than low frequency components. A loading process of high strain rate contains more high frequency components, so it activates smaller cracks in a concrete specimen.

The above discussion leads to the concept that more cracks with a smaller average size are developed by high strain rate loading. Meanwhile, as discussed previously, the dynamic increase factor is also correlated to the strain rate similarly. So, it is reasonable to assume that the number of cracks within the unit volume can be expressed as a linear function of the dynamic increase factor in tension (TDIF) as described in Eqs. (2a) to (2c)

$$N = \alpha f(\dot{\varepsilon}) \tag{8}$$

where $f(\dot{\varepsilon}) = TDIF$, as given in Eqs. (2a) to (2c), α is a material parameter. The physical meaning of α is the number of cracks within the unit volume when material fails under static condition.

According to the principle of fracture mechanics, the increasing rate of the crack radius is related to the stress intensity factor and its increasing rate by

$$\dot{r} = \eta c K^{\eta-1} \dot{K} \tag{9}$$

where K is the stress intensity factor, and c and η are parameters. Stress intensity factor can be expressed in terms of the damage energy release rate (G) and Young's modulus (E) as $K = \sqrt{EG}$, or in an incremental format of $\dot{K} = \frac{1}{2} E^{\frac{1}{2}} G^{-\frac{1}{2}} \dot{G}$. The increasing rate of the spherical reign surrounding the crack is then expressed as

$$\dot{V} = 4\pi r^2 \dot{r} \tag{10}$$

Thus, the incremental tensile damage (D) is

$$\dot{D} = 2\pi\eta c^2 \alpha f(\dot{\varepsilon}) E^{\eta-1} G^{\eta-\frac{1}{2}} \dot{G} \tag{11}$$

As discussed by Lemaitre (1992), $\dot{G}$ can be replaced approximately by the rate of accumulated plastic strain when material is under compression. When concrete is under tension, the damage is brittle, $\dot{G}$ is correlated linearly with the relative buck strain rate of the material, $\dot{\varepsilon}_v$ (Zhao 2003). By replacing G with K_{IC}^2/E and combining all material parameters and in Eq. (11), the incremental tensile damage is

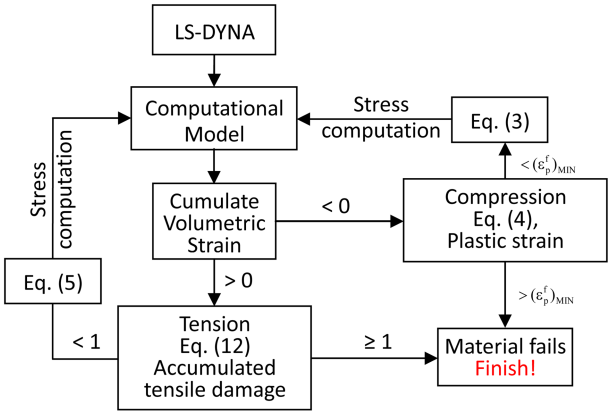

Fig. 2 Computational flowchart

$$\dot{D} = \zeta \cdot f(\dot{\varepsilon}) E^{-\frac{1}{2}} K_{IC}^{2\eta-1} \dot{\varepsilon}_v \tag{12}$$

2.4 Failure criterions

Two failure criteria, compression and tension, are employed in this study. Same criterion as used in the HJC model is applied for compression failure of concrete. The maximum equivalent plastic strain at fracture is set as a critical value. If the probe stress of an element exceeds the strength of the material, plastic deformation occurs. When the cumulated equivalent plastic strain exceeds the maximum equivalent plastic strain at fracture, then material is damaged and the elements are removed from the model by erosion algorithm. Concrete experiences brittle tension damage, and it is controlled by the tensile damage scalar D_T. When accumulated tension damage exceeds the critical value, then material fails and the elements are removed from the model. The proposed material model described in previous section was incorporated into the commercial software LS-DYNA, through the user defined materials function. The flowchart for the computation is shown in Fig. 2.

3. Numerical simulations

3.1 Model descriptions

The present material model was applied to simulate the tests of rigid bullet impact on concrete targets conducted by the author and other researchers (Zhang 2005). In that experimental study, all specimens subjected to impact tests had a common size of 300 × 170 mm and a thickness of 150 mm with concrete compressive strengths of 45-C235 MPa. A 12.6 mm ogive-nosed projectile was used to hit the concrete target at the center at velocities ranging from 620 to 700 m/s. Due to symmetry, a quarter of the target and projectile is modeled, as shown in Fig. 3. Since no damage is observed on projectiles after all impact tests, the rigid material model (#20 in LS-DYNA) was used for the steel projectile. The material density and elastic modulus of the target steel are 7500 kg/m^3 and 2.1E+11Pa, respectively. The parameters of concrete used in this study are obtained from a

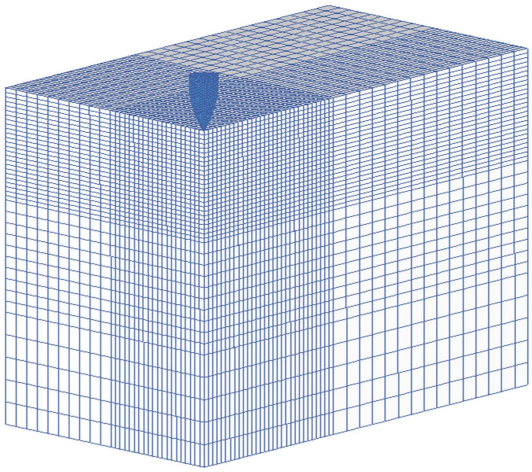

Fig. 3 FE model

Table 1 Simulation parameters for different cases (Zhang 2005)

Case number	Specimen designation	Fiber contain (%)	f_c' (MPa)	f_t (MPa)	Impact velocity (m/s)	Crater diameter (mm)	Penetration depth (mm)
Case 1	CM-150	0	151	13	647	125	31
Case 2	QOF-1-2	1.5	204	33	645	85	31

Table 2 Basic material parameters for concrete

Case number	ρ (kg/m^3)	E (GPa)	K (GPa)	G (GPa)	ν
Case 1	2.419	20.7	9.5	8.5	0.18
Case 2	2.502	39.3	16.0	15.0	0.20

Table 3 Basic damage parameters for concrete, Case 1

A	B	N	D_1	D_2	EF_{MIN}	S_{max}	ζ	K_{IC} (MPam$^{0.5}$)	η
0.8	1.6	0.6	0.04	1.0	0.01	7	0.45	2.5	0.01

Table 4 Basic damage parameters for concrete, Case 2

A	B	N	D_1	D_2	EF_{MIN}	S_{max}	ζ	K_{IC} (MPam$^{0.5}$)	η
0.8	1.2	0.4	0.04	1.0	0.01	7	0.45	5.0	0.01

previous study on the compressive and tensile dynamic behavior of concrete; and typical material parameters for plain and fiber reinforced concrete and impact velocities used in this study were summarized in Table 1 (Zhang 2005).

The target-projectile system is established in the Lagrange coordinate system. The standard algorithm "eroding surface-to-surface" contact interface is adopted. The Flanagan-Belytschko stiffness, based

on hourglass control, is implied for target elements. In the present study, the strain failure criterion was also used as an element erosion criterion.

3.2 Numerical results and discussion

Tensile and compressive damage contour distributions in the target at different stages of impact are shown in Figs. 4 and 5. At the early stage of the penetration process, the extrusion dilation of the target material is found, due to the high speed of the projectile. As the penetration depth increases and the projectile speed decreases, the ranges of damage decrease gradually. The compressive damage appears in the area immediately in front of and surrounding the projectile, while the tensile damage area distributes around the impact center. The tensile damage contour shows a clear trend of how the crater happens.

Fig. 6 indicates the contours of von-Mises effective stress, which reflects the asymmetric stress wave during the process of projectile penetration. It can be seen the effective stress near the front of the projectile head is larger than those at other locations. The propagation of stress wave in the concrete targets is clearly presented. The dissipation of the stress wave was observed as the stress wave transmitted in the targets. Fig. 7 compares the simulation results with the experimental data obtained by the authors in a previous study (Zhang 2005). The average crater diameter from simulation Case 1 and 2 are 105 mm and 75 mm, respectively, which are comparable with the experimental results, 125 mm and 85 mm. It is also noticed that the shape of the front damage and

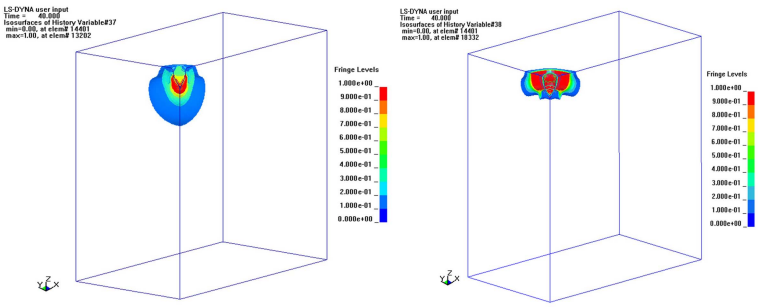

(a) Compressive damage contour (b) Tensile damage contour

Fig. 4 Damage in the middle of impact (t = 40 us)

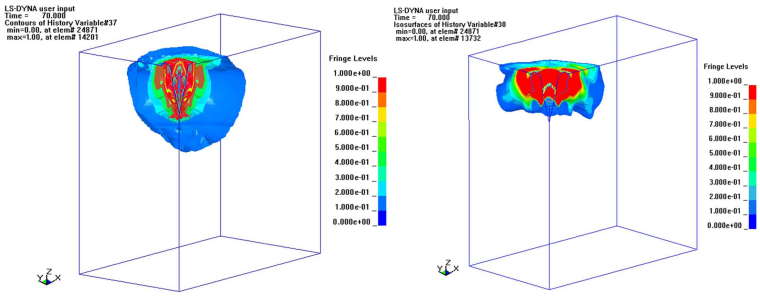

(a) Compressive damage contour (b) Tensile damage contour

Fig. 5 Damage at end of the impact (t = 70 us)

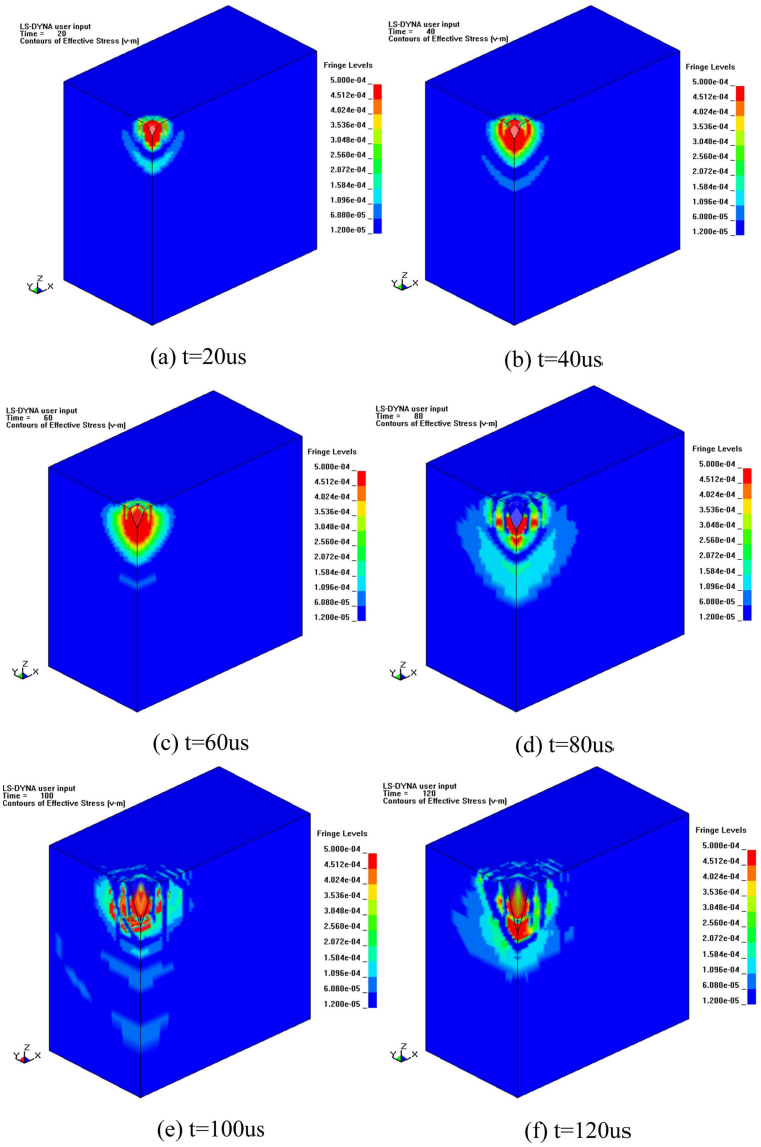

Fig. 6 Contours of von-Mises effective stress in the target (unit:100 GPa)

cracking predicted in numerical simulations are similar to the real damage on concrete front surface right under impact. The numerical simulations using the presented material model provide a reasonable prediction on the front damage of the concrete targets.

Even though in the present study the concrete targets were massive blocks and the penetration does not occur, the compressive stiffness loses when loads are revered due to the removal of the elements. It should be noted that the element erosion is a numerical consideration and not as same as the material failure. It should also be noted that penetration and perforation tests give complex state of stress, and because tensile and compression waves act always on the specimens, reversal loading situations are expected in the material. Under impact, materials next to the surfaces will

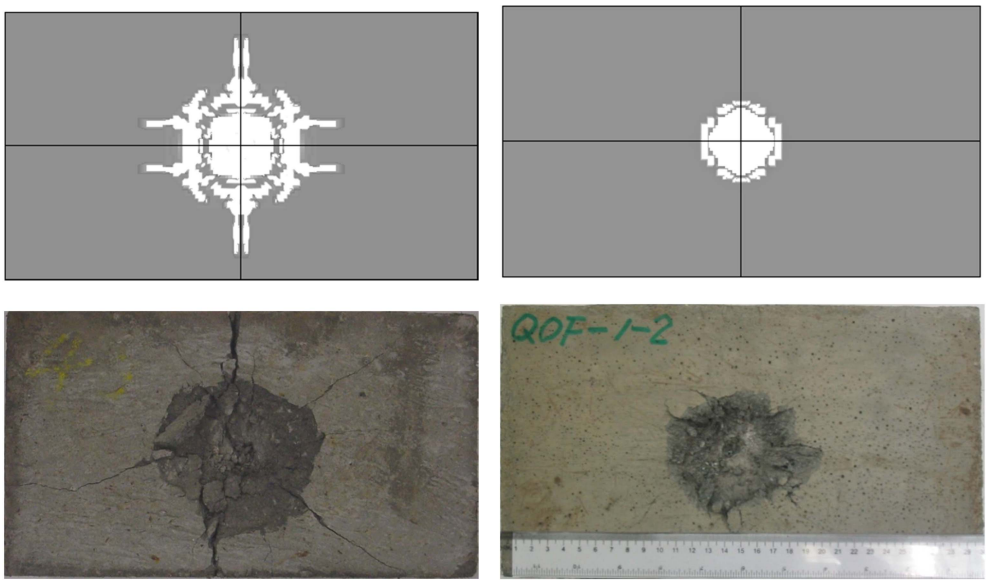

(a) Plain concrete target (case 1) (b) Fiber reinforced concrete target (case 2)

Fig. 7 Comparison of the numerical and experimental results

experiment tensile cracking (e.g. spalling, scabbing) due to tensile waves. Moreover, the extrim pressure right beneath and surounding the projectile nose makes target elements undergo large element distortion, which requires a very small time step. Under these considerations the mesh size and erosion criteria will play more critical roles in the numerical simulation. Normally, the size of the target elements right under and surrounding impact shall be small enough to achieve an accurate simulation. However, further reduced element size won't affect the simulation results significantly (Islam *et al*. 2011).

4. Conclusions

The mechanism of front damage of the fiber-reinforced concrete target under projectile impact was investigated, based on experimental observations. Furthermore, a modified material model for both plain and fiber-reinforced concrete, based on the HJC constitutive model, is developed and incorporated into the LS-DYNA code. The material model developed in this study includes ten material parameters, and is of the capability to describe both compressive and tensile damages and strain rate effect.

Numerical simulations are performed, by using this modified material model with experimental data obtained by these authors. The results are in good agreement with experimental observations. From the numerical simulations, the process of the front face damage of the concrete target is clearly presented. The damage is a combined effect of compression and tension failure of the material. At the early stage of impact, damage is concentrated in a small area immediately in front of the tip of the projectile. Crushing of concrete materials is the only mode of damage. As the projectile moves into concrete, splitting cracks may appear, as well as dust ejection, due to crushed fragmentation of concrete materials.

References

Bischoff, P.H. and Perry, S.H. (1991), "Compressive behaviour of concrete at high strain rate", *Mater. Struct.*, **24**, 425-450.

Bindiganavile, V., Banthia, N. and Aarup, B. (2002), "Impact response of ultra-high strength-reinforced cement composite", *ACI Mater. J.*, **99**(6), 543-548.

Cao, J. and Chung, D.D.L. (2002), "Effect of strain rate on cement mortar under compression, studied by electrical resistivity measurement", *Cement Concrete Res.*, **32**, 817-819.

Clifton, J.R. (1982), *Penetration resistance of concrete-a review*, National Bureau of Standards Special Publication, Washington D.C., 480-485.

Collins, A., Chapman, D. and Proud, W. (2007), "Shock compression of condensed matter", *AIP Conference Proceedings*, **955**, 497-500.

Cotsovos, D.M. and Pavlovic, M.N. (2008), "Numerical investigation of concrete subjected to compressive impact loading. Part 1: A fundamental explanation for the apparent strength gain at high loading rates", *Comp. Struct.*, **86**, 145-163.

Cotsovos, D.M. and Pavlovic, M.N. (2008), "Numerical investigation of concrete subjected to compressive impact loading. Part 2: Parametric investigation of factors affecting behaviour at high loading rates", *Comp. Struct.*, **86**, 164-180.

Cotsovos, D.M. and Pavlovic, M.N. (2008), "Numerical investigation of concrete subjected to high rates of uniaxial tensile loading", *Int. J. Impact Eng.*, **35**, 319-335.

Dancygier, A.N. and Yankelevsky, D.Z. (1996), "High strength concrete response to hard projectile impact", *Int. J. Impact Eng.*, **18**(6), 583-599.

Dancygier, A.N. and Yankelevsky, D.Z. (2002), "Penetration mechanisms of non-deforming projectiles into reinforced concrete barriers", *Struct. Eng. Mech.*, **13**, 171-186.

Degen, P.P. (1980), "Perforation of reinforced concrete slab by rigid missiles", *J. Struct. Div. - ASCE*, **106**(7), 1623-1642.

Forrestal, M.J. and Luk, V.K. (1988), "Dynamic spherical cavity expansion in a compressible elastic plastic solid", *J. Appl. Mech.*, **55**, 275-279.

Gebbeken, N. and Ruppert, M. (2000), "A new material model for concrete in high-dynamic hydrocode simulations", *Arch. Appl. Mech.*, **70**, 463-478.

Grady, D.E. and Kipp, M.E. (1980), "Continuum modeling of explosive fracture in oil shale", *Int. J. Rock Min. Sci.*, **17**, 147-157.

Hanchak, S.J., Forrestal, M.J., Young, E.R. and Ehrgott, J.Q. (1992), "Perforation of concrete slabs with 48 MPa (7 ksi) and 140 MPa (20 ksi) unconfined compressive strengths", *Int. J. Impact Eng.*, **12**(1), 1-7.

Holmquist, T.J., Johnson, G.R. and Cook, W.H. (1993), "A computational constitutive model for concrete subjected to large strains, high strain rates and high pressures", *Proc. 14th Int. Sym. Ball*, Quebec, Canada, 591-600.

Islam, M.J., Liu, Z. and Swaddiwudhipong, S. (2011), "Numerical study on concrete penetration/perforation under high velocity impact by ogive-nose steel projectile", *Comput. Concrete*, **8**(1), 111-123.

van Mier, J.G.M. (1997), *Fracture processes of concrete*, CRC Press, ISBN:0-8493-9123-7, 284-285.

Lemaitre, J. (1992), *A course on damage mechanics*, Springer-Verlag Press, ISBN:3-540-53609-4.

Leppänen, J. (2006), "Concrete subjected to projectile and fragment impacts: modelling of crack softening and strain rate dependency in tension", *Int. J. Impact Eng.*, **32**, 1828-1841.

Li, X.B. and Gu, D.S. (1994), *Rock impact dynamics,* Central South University of Technology Press, China, ISBN:7-81020-670-2/TD.034.

Lok, T.S., Zhao, P.J. and Lu, G. (2003), "Using the split Hopkinson pressure bar to investigate the dynamic behaviour of SFRC", *Mag. Concrete Res.*, **55**(2), 183-191.

LS-DYNA Keyword User's Manual Ver. 950 (1999), *Livermore software technology corporation*, LSCT.

Luk, V.K. and Forrestal, M.J. (1987), "Penetration into semi-infinite reinforced concrete target with spherical and ogival nose projectiles", *Int. J. Impact Eng.*, **6**(4), 291-301.

Malvar, L.J. and Ross, C.A. (1998), "Review of strain rate effects for concrete in tension", *ACI Mater. J.*, **95**(6), 735-739.

Mehta, P.K. and Monteriro P.J.M. (2006), *Concrete microstructure, properties, and materials*, McGraw-Hill, New York, 612-627.
O'Neil, E.F., Neeley, B.D. and Cargile, J.D. (1999), "Tensile properties of very-high-strength concrete for penetration-resistant structures", *Shock. Vib.*, **6**(5), 237-245.
Ou, Z., Duan, Z. and Huang, F. (2010) "Analytical approach to the strain rate effect on the dynamic tensile strength of brittle materials", *Int. J. Impact Eng.*, **37**, 942-945.
Polanco-Loria, M., Hopperstad, O.S., Børvik, T. and Berstad, T. (2008), "Numerical predictions of ballistic limits for concrete slabs using a modified version of the HJC concrete model", *Int. J. Impact Eng.*, **35**, 290-303.
Riedel, W., Thoma, K., Hiermaier, S. and Schmolinske, E. (1999), "Penetration of reinforced concrete by BETA-B-500 numerical analysis using a new macroscopic concrete model for hydrocodes", *Proc. 9th Int. Sym. Interaction of the Effects of Munitions with Structures*, Berlin, Germany, 315-322.
Ross, C.A., Jerome, D.M., Tedesco, J.W. and Hughes, M.L. (1996), "Moisture and strain rate effects on concrete strength", *ACI Mater. J.*, **93**(3), 293-300.
Schuler, H., Mayrhofer, C. and Thoma, K. (2006), "Spall experiments for the measurement of the tensile strength and fracture energy of concrete at high strain rates", *Int. J. Impact Eng.*, **32**(10), 1635-1650.
Shockey, D.A., Curran, D.R., Seaman, L., Rosenberg, J.T. and Petersen, D.F. (1974), "Fragmentation of rock under dynamic loads", *Int. J. Rock. Mech. Min. Sci. Geomech.*, **11**, 303-317.
Suaris, W. and Shah, S.P. (1984), "A rate sensitive damage theory for brittle solids", *J. Eng. Mech. - ASCE*, **110**(6), 985-997.
Taylor, L.M., Chen, E.P. and Kuszmaul, J.S. (1986), "Microcrack-induced damage accumulation in brittle rock under dynamic loading", *Comput. Method. Appl. M.*, **55**, 301-320.
Zhao, P.J. (2003), "The split Hopkinson pressure bar for testing concrete and steel fibre reinforced concrete", Ph.D. Thesis, Nanyang Technological University, Singapore.
Zhang, M.H., Sharif, M.S.H. and Lu, G. (2007), "Impact resistance of high-strength fibre reinforcedconcrete", *Mag. Concrete Res.*, **59**(3), 199-210.
Zhang, M.H., Shim, V.P.W., Lu, G. and Chew, C.W. (2005), "Resistance of high-strength concrete to projectile impact", *Int. J. Impact Eng.*, **31**(7), 825-841.
Zhou, X.Q., Kuznetsov, V.A., Hao, H. and Waschl, J. (2008), "Numerical prediction of concrete slab response to blast loading", *Int. J. Impact Eng.*, **35**(10), 1186-1200.

CC